Principal Component Regularization in Iterative Inversion of DBIM for Ultrasound Tomography

Nguyen Thi Thu
Faculty of Embedded Systems and Integrated Circuits, School of Electrical and Electronic Engineering, Hanoi University of Industry, Hanoi, Vietnam
thunt@haui.edu.vn

Tran Quang-Huy*
Faculty of Physics Hanoi Pedagogical University 2, Hanoi, Vietnam
tranquanghuy@hpu2.edu.vn

Luong Thi Theu
Hoa Binh University, Hanoi, Vietnam
lttheu@daihochoabinh.edu.vn

Duc-Tan Tran
Faculty of Electrical and Electronic Engineering, Phenikaa University, Hanoi 12116, Vietnam
tan.tranduc@phenikaa-uni.edu.vn

***Abstract*— In this study, we propose an improved framework for ultrasound tomographic image reconstruction by incorporating principal component analysis (PCA) into the iterative process of the distorted Born iterative method (DBIM). While traditional DBIM is effective in solving inverse scattering problems, it often exhibits slow convergence and poor performance under noisy conditions due to the accumulation of high-variance noise components across iterations. To overcome this, we embed a PCA-based filtering step into each iteration, which adaptively retains the most informative components of the current reconstruction and suppresses noise-dominated directions. Numerical simulations under varying problem sizes, with a fixed number of measurements, demonstrate that the PCA-enhanced DBIM significantly reduces the normalized reconstruction error—achieving up to 36% error reduction compared to standard DBIM—and exhibits faster convergence, particularly in underdetermined scenarios. These results confirm that PCA not only improves the stability and robustness of the inversion process but also serves as an effective spatial regularizer, making it a promising tool for enhancing the quality and efficiency of iterative acoustic imaging methods.**

Keywords*— *Ultrasound tomography, distorted born iterative method (DBIM), principal component analysis (PCA), image reconstruction, noise suppression.

I. Introduction

Since the emergence of sonar technology, sound wave-based imaging methods have been widely adopted in various domains, particularly in biomedical applications. Among these, B-mode ultrasound imaging [1] stands as the cornerstone of clinical sonography due to its simplicity, real-time feedback, and non-ionizing nature. It visualizes anatomical structures by mapping acoustic impedance contrasts, allowing clinicians to identify tissue boundaries and lesions. However, as a qualitative imaging modality, B-mode lacks quantitative representation of tissue properties, resulting in a strong dependence on the experience and subjective interpretation of medical professionals, which can lead to inconsistent diagnostic outcomes. To overcome these limitations, ultrasound tomography (UST) has been developed as a powerful tool to reconstruct quantitative distributions of acoustic parameters such as sound speed, attenuation, and density [2], [3]. Unlike conventional reflection-based techniques, UST relies on transmission and scattering measurements to solve an inverse problem that links the acoustic wavefield to the internal properties of the medium. This provides the foundation for quantitative imaging, where the goal is not merely to visualize structures, but to characterize them physically. Such a capability is of significant interest in applications like tumor detection, breast tissue classification, and liver fibrosis assessment.

The theoretical foundation of UST often adopts first-order linear approximations, namely the Born approximation [4] and Rytov approximation [5], to linearize the otherwise nonlinear wave equation. These approximations assume that the medium perturbations are weak enough to neglect multiple scattering effects, thereby enabling efficient inversion. However, when imaging complex biological tissues where scattering is strong, the first-order models become inadequate, leading to inaccurate reconstructions. To tackle this, more advanced iterative inversion schemes have been proposed, most notably the born iterative method (BIM) and its extension, the distorted born iterative method (DBIM) [6], [7]. DBIM improves upon BIM by updating the Green's function at each iteration to account for the current estimate of the scattering potential, thereby capturing moderate to strong scattering effects more accurately. These methods are well-regarded for their ability to recover fine-scale features in acoustic profiles, yet they come at a cost: the inverse problem is highly ill-posed, computationally demanding, and extremely sensitive to measurement noise.

Several strategies have been explored to reduce the computational burden and enhance robustness of DBIM. These include algorithmic acceleration methods, regularization techniques, and hybrid inversion frameworks that combine model-based and data-driven components [8]–[11]. While such approaches improve performance to a degree, the persistent challenge remains the contamination of scattered field data by Gaussian thermal noise and speckle noise, which is especially problematic in low signal-to-noise ratio (SNR) settings common in biomedical scenarios. If the raw noisy data is directly input into the DBIM algorithm, the noise not only corrupts the initial estimates but may also accumulate and amplify over successive iterations, resulting in

979-8-3315-7206-8/25/$31.00

distorted reconstructions and spurious artifacts. Therefore, effective noise suppression is not merely beneficial—it is imperative. Prior works have approached this through multi-frequency excitation strategies [12]–[15], wherein imaging is performed sequentially across a range of frequencies. This spectral diversity enhances spatial resolution and mitigates frequency-dependent noise artifacts. The underlying principle is that low-frequency waves provide global structural information with high penetration, while high-frequency waves offer finer detail. By integrating these multi-scale reconstructions, a more robust and high-fidelity image can be obtained. Despite their advantages, multi-frequency methods suffer from increased acquisition time, hardware constraints, and limited efficacy when the noise spectrum overlaps with the signal spectrum across frequencies. Furthermore, they often treat denoising as an external preprocessing or postprocessing step, rather than integrating it within the inversion loop.

To address these shortcomings, we propose a novel framework that integrates principal component analysis (PCA) as a regularization and denoising mechanism within each DBIM iteration. PCA is a statistical method that transforms the original signal space into an orthogonal basis where the principal components are ordered by their variance. In the context of image reconstruction, this allows for decomposition of the estimated image into dominant signal modes and low-energy components typically associated with noise. By adaptively retaining only the principal components that capture significant structural content, PCA serves to suppress stochastic noise while preserving salient anatomical features. Our approach departs from conventional methods in that denoising is embedded directly into the iterative inversion pipeline, allowing the algorithm to benefit from noise suppression at every update step. This integration helps to stabilize the inversion process, prevent error propagation, and accelerate convergence, thereby achieving better reconstructions with fewer iterations. The proposed PCA-enhanced DBIM framework is particularly attractive for applications where measurement conditions are suboptimal, or when computational efficiency is essential, such as point-of-care diagnostics and portable imaging systems.

II. Methodology

The imaging configuration considered in this study consists of multiple ultrasonic transmitters and receivers uniformly distributed along the perimeter of a circular scanning region, as illustrated in Fig. 1. The acquired scattering data is processed through the DBIM framework to iteratively estimate the perturbation in acoustic parameters, particularly variations in sound velocity and tissue density.

In the assumed scenario, an inhomogeneity—representing, for instance, a tumor—is embedded in a homogeneous background medium such as water. This object, denoted as $O(r)$, differs acoustically from the background due to its contrast in sound speed. Let N_t be the number of transmitters and N_r the number of receivers. During acquisition, each transmitter is activated sequentially, while all receivers simultaneously record the resulting scattered pressure field. For each transmission event, N_r measurements are obtained, yielding a total dataset of size $N_t \times N_r$ after all transmissions are completed.

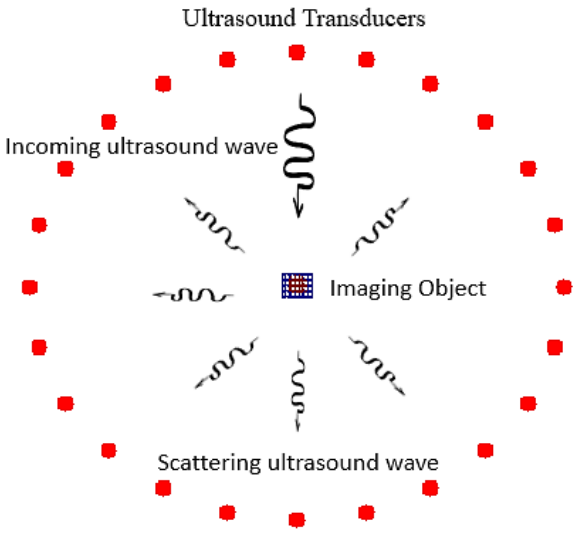

Fig. 1. Measurement setup for DBIM-based ultrasound tomography.

The acoustic contrast is mathematically represented by the object function:

$$H(\vec{r}) = \begin{cases} \omega^2 \left(\frac{1}{c_1^2} - \frac{1}{c_0^2}\right), \vec{r} \le R \\ 0, \ \vec{r} > R \end{cases}, \quad (1)$$

where c_1 and c_0 are the sound speeds in the object and background medium, respectively, ω is the angular frequency of the wave, and R is the radius of the object.

The total acoustic pressure at a point in the field can be written as:

$$A(\vec{r}) = A^{inc}(\vec{r}) + A^{sc}(\vec{r}), \quad (2)$$

where $A^{inc}(\vec{r})$ is the incident pressure, and $A^{sc}(\vec{r})$ is the pressure scattered by the object. In integral form, this becomes:

$$A(\vec{r}) = A^{inc}(\vec{r}) + \iint H(\vec{r'})A(\vec{r'})G_0(|\vec{r} - \vec{r'}|)d\vec{r'}, \quad (3)$$

where $G_0(.)$ is the Green's function in a homogeneous medium. Discretizing this formulation, the scattered pressure data vector $\bar{A}^{sc}$ of size $N_t N_r \times N^2$ is given by:

$$\bar{A}^{sc} = \bar{B}.D(\bar{H}).\bar{A} = \bar{M}\bar{H}, \quad (4)$$

where $\bar{M} = \bar{B}.D(\bar{A})$ is the system matrix, $\bar{B}$ represents the Green's coefficients from each pixel to the receivers, $\bar{C}$ represents the matrix with Green's coefficient $G_0(r, r')$ among

all pixels, $\bar{I}$ is an identity matrix, and D(·) is the operator converting a vector into a diagonal matrix.

The measured scattered signal $\bar{A}^{sc}$, however, is typically corrupted by Gaussian noise, which can degrade the accuracy of the reconstruction if not addressed effectively. To overcome this, we propose the use of principal component analysis (PCA) as an integrated denoising strategy within each iteration of DBIM. Rather than processing noise as a preprocessing step, PCA is applied to the scattered pressure data during every iteration of the inversion loop.

In this framework, PCA is used to project the scattered field $\bar{A}^{sc}$ onto a lower-dimensional subspace spanned by its leading principal components. These components capture the most significant spatial structures of the acoustic field, while noise—typically residing in the low-variance components—is filtered out. This dimensionality-reduced signal is then passed into the DBIM update step, leading to a more stable inversion process.

The detailed reconstruction procedure is summarized in Algorithm 1.

Algorithm 1. PCA-enhanced DBIM reconstruction

Set initial guess $\bar{H}_{(0)}$, and compute incident field $\overline{A}^{inc}$ using Eq. (5)
Compute Green's matrices $\bar{B}$ and $\bar{C}$
For $n = 1\ to\ N$ (maximum iterations), do
1. Compute scattered field $\bar{A}^{sc}$ using Eq. (4)
2. Apply PCA to $\bar{A}^{sc}$ and retain leading components
3. Update estimate $\bar{H}_{(n+1)}$ via Tikhonov regularization
4. n = n + 1
End For

The incident field for a zero-order Bessel beam in 2D is computed as:

$$\overline{A}^{inc} = J_0(k_0|r - r_k|), \tag{5}$$

where J_0 is the Bessel function of the first kind (order zero), and r_k denotes the location of the kth transmitter.

This PCA-integrated DBIM framework offers several advantages: it suppresses noise adaptively at each iteration, reduces error accumulation, and accelerates convergence by focusing reconstruction updates on the most informative components of the scattered field. Compared to LMS filtering, PCA does not rely on filter tuning parameters or convergence heuristics, and it requires no prior knowledge of noise statistics, making it particularly suitable for biomedical imaging environments with variable noise conditions.

III. Simulation And Results

To evaluate the performance of the proposed PCA-regularized DBIM method, a set of controlled numerical experiments was conducted using a circular imaging domain. The acoustic wave frequency was set to 1MHz, which corresponds to a typical operating range for soft tissue ultrasound tomography and provides a balance between penetration depth and spatial resolution. The region of interest (ROI) was discretized into a uniform N×N pixel grid, yielding a total of N^2 variables to be reconstructed. The scattering region, which simulates an inhomogeneous object (e.g., a tumor or lesion), was modeled as a circular inclusion embedded in a homogeneous background medium. The diameter of this inclusion was fixed at 10 mm, and the acoustic contrast—defined as the relative difference in sound speed between the object and the background—was set to 30%, a representative value for soft tissue anomalies. The measurement geometry included 22 transmitters and 12 receivers, resulting in N_t = 22 and N_r = 12, respectively. Both transmitters and receivers were placed evenly on a circular ring surrounding the imaging domain. The distance from each transmitter and receiver to the center of the ROI was set to 100 mm. To simulate realistic measurement conditions, Gaussian noise was introduced into the scattered pressure field, with its standard deviation set to 10% of that of the original noise-free signal.

Figure 2 illustrates the ideal object function, representing the ground truth distribution of the acoustic contrast within the imaging domain. This serves as a reference for evaluating the reconstruction quality of the tested algorithms. Figure 3 presents the reconstructed images obtained using the standard DBIM method after the first (a), third (b), and fifth (c) iterations, corresponding to the case with N=18. The progression of the reconstruction demonstrates gradual refinement of the object's shape and contrast, though residual noise remain noticeable, especially in the early iterations. Figure 4 shows the corresponding reconstructions using the proposed PCA-enhanced DBIM, again after the first (d), third (e), and fifth (f) iterations, with the same N=18. Visually, the reconstructions obtained from the proposed PCA-enhanced DBIM exhibit notably reduced background noise compared to those from the standard DBIM. At each iteration, the reconstructed object using PCA filtering appears more consistent with the ideal object function, with fewer artifacts and improved contrast. By the fifth iteration (f), the PCA-based reconstruction closely resembles the ground truth suggesting superior noise suppression and faster convergence. These visual observations clearly demonstrate the advantage of integrating PCA into the iterative inversion process, leading to more stable and accurate ultrasound image reconstruction.

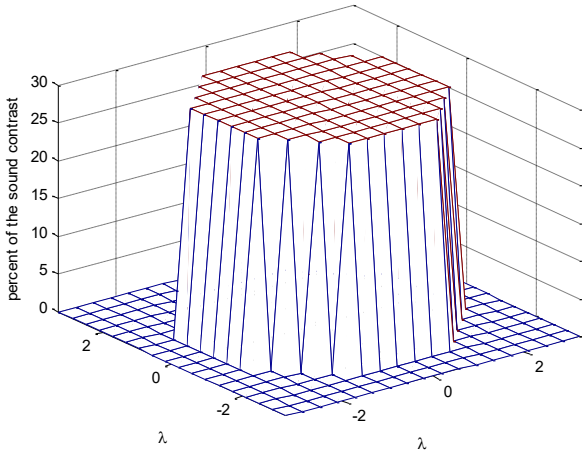

Fig. 2: Ideal object function.

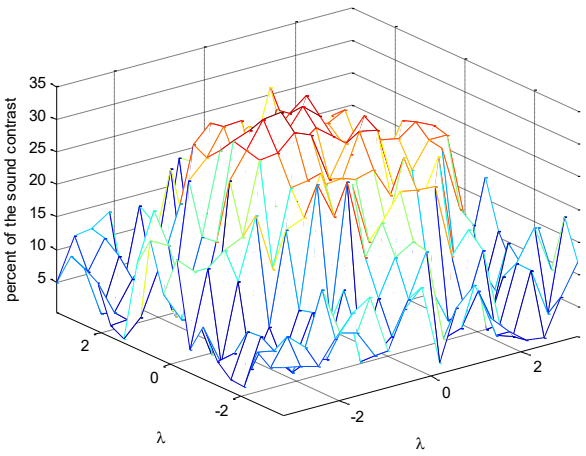

(a)

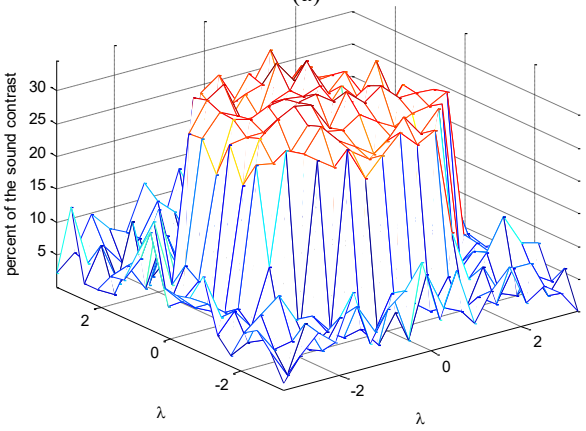

(b)

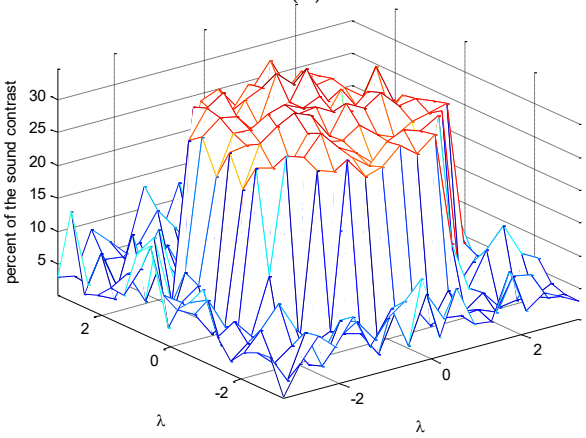

(c)

Fig. 3: Reconstructed object by the DBIM after first (a), third (b) and fifth (c) iterations (with the case of N=18).

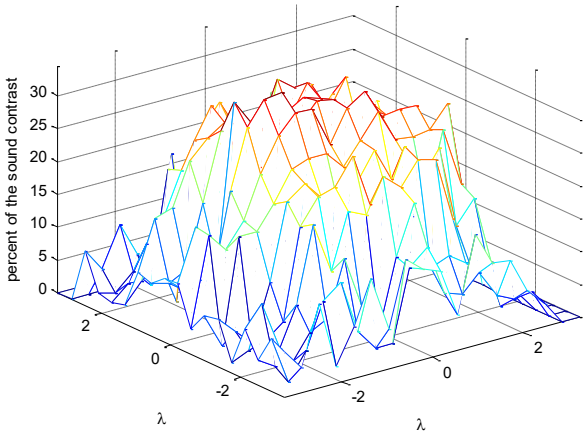

(d)

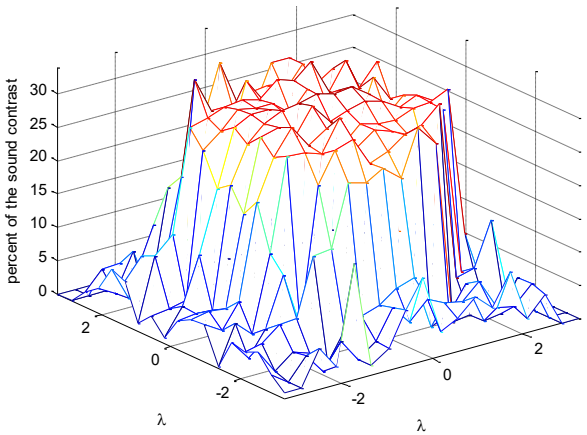

(e)

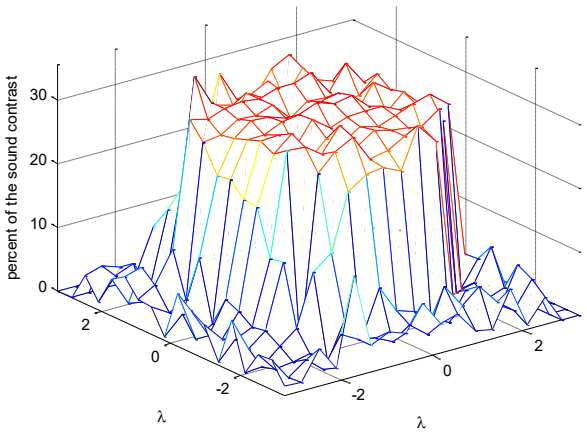

(f)

Fig. 4: Reconstructed object by the PCA-enhanced DBIM after first (d), third (e) and fifth (f) iterations (with the case of N=18).

To quantitatively evaluate the performance of the proposed method, the discrepancy between the filtered signal and the original uncorrupted signal is measured. Let $m \in R^{V \times W}$

denote the original signal, and let $\hat{m}$ represent the corresponding filtered (denoised) signal. The accuracy of the filtering process is assessed using the relative residual error (RRE), which is defined as:

$$\varepsilon = \frac{1}{V \times W} \sum_{i=1}^{V} \sum_{j=1}^{W} \frac{\left| m_{ij} - \hat{m}_{ij} \right|}{\left| m_{ij} \right|} \tag{6}$$

In our numerical simulation, the number of measurements was fixed at 264 (22 transmitters × 12 receivers), while the number of unknowns was gradually increased from 324 to 900, allowing us to investigate the performance of PCA-DBIM under increasingly ill-posed conditions. The normalized reconstruction error was recorded after each of five iterations for both standard DBIM and the proposed PCA-enhanced DBIM as shown in Table 1.

At 324 variables, the PCA-DBIM already shows noticeable advantages as shown in Fig. 5(a). While both methods reduce the error over iterations, PCA-DBIM converges faster and achieves a significantly lower final error (0.2028 vs 0.3152), corresponding to a 35.7% relative reduction. The improvement is also visible as early as the third iteration, where PCA-DBIM attains 0.2536 versus 0.3368 for DBIM, indicating early-stage convergence acceleration due to PCA filtering. As the number of variables increases to 400, the standard DBIM struggles to significantly improve beyond the third iteration, stagnating around 0.4317, while PCA-DBIM continues to reduce the error down to 0.3449 by the fifth iteration—yielding a 20.1% improvement. This demonstrates PCA's capability to regularize the inversion path, enabling continued progress even when DBIM reaches a local plateau. At 484 variables, PCA-DBIM further improves performance. The final error reduces from 0.4493 (DBIM) to 0.3285 (PCA-DBIM), a 26.9% decrease. In particular, PCA suppresses noise components effectively, allowing for more stable inversion steps. This behavior aligns with the mathematical nature of PCA, which retains dominant eigen-directions corresponding to structural information and discards low-variance noise components that often disrupt iterative updates.

As we move to larger problems, such as 576 variables, the trend remains consistent as shown in Fig. 5(b): PCA-DBIM achieves a final normalized error of 0.3525, compared to 0.5020 for DBIM—representing a 29.8% error reduction. Moreover, from iteration 2 onward, PCA-DBIM consistently outperforms DBIM, which becomes increasingly trapped in noisy reconstructions. Even at 676 variables, PCA continues to outperform DBIM with a 33.4% improvement in the final error (from 0.4966 to 0.3308). This robustness under increased ill-posedness shows the strength of PCA as an implicit dimensionality-reduction technique, helping to mitigate instability arising from limited measurements. At the upper end of the spectrum—784 and 900 variables—both methods exhibit degraded performance due to the severe underdetermination (i.e., far more unknowns than measurements). Nevertheless, PCA-DBIM consistently maintains an advantage. At 900 variables as shown in Fig. 5(c), the final normalized error is 0.4151 with PCA, versus 0.5554 for DBIM, yielding a 25.3% relative reduction. Although the overall reconstruction quality worsens with more unknowns, PCA still acts as an effective spatial filter that guides the inversion toward the signal-dominant subspace, thereby maintaining greater stability.

In summary, across all tested problem sizes, PCA-DBIM not only reduces the normalized reconstruction error significantly (with improvements ranging from 20% to nearly 36%) but also accelerates convergence. These improvements stem from PCA's ability to suppress noise accumulation by retaining only the most informative components of the reconstructed image during each iteration. As a result, the integration of PCA into DBIM proves especially valuable in underdetermined scenarios, enhancing both reconstruction accuracy and algorithmic stability.

Tab. 1. Normalized reconstruction error after each iteration for DBIM and PCA-DBIM with varying numbers of unknown variables (measurements fixed at 264)

Number of varibles	Methods	Normalized error after every iteration				
324	DBIM	0.5872	0.3862	0.3368	0.3216	0.3152
	PCA-DBIM	0.4901	0.3146	0.2536	0.2210	0.2028
400	DBIM	0.6145	0.4618	0.4387	0.4333	0.4317
	PCA-DBIM	0.6650	0.4443	0.3859	0.3597	0.3449
484	DBIM	0.6644	0.4812	0.4544	0.4506	0.4493
	PCA-DBIM	0.5689	0.4037	0.3579	0.3375	0.3285
576	DBIM	0.6847	0.5341	0.5064	0.5027	0.5020
	PCA-DBIM	0.5901	0.4611	0.4049	0.3738	0.3525
676	DBIM	0.6000	0.5082	0.4992	0.4973	0.4966
	PCA-DBIM	0.5307	0.4138	0.3687	0.3452	0.3308
784	DBIM	0.6577	0.5510	0.5416	0.5404	0.5402
	PCA-DBIM	0.6512	0.5271	0.4867	0.4675	0.4566
900	DBIM	0.6822	0.5691	0.5570	0.5556	0.5554
	PCA-DBIM	0.6151	0.4997	0.4549	0.4305	0.4151

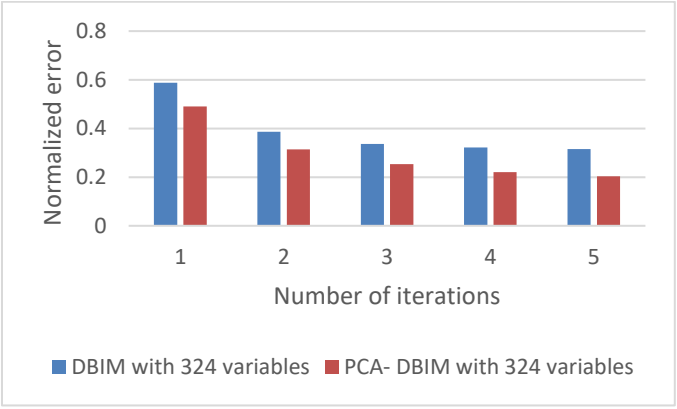

(a)

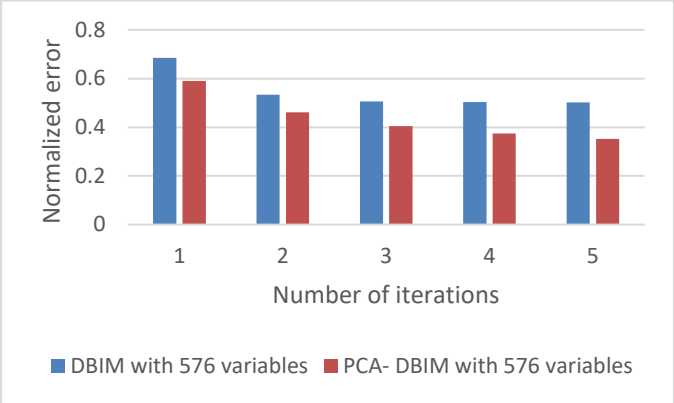

(b)

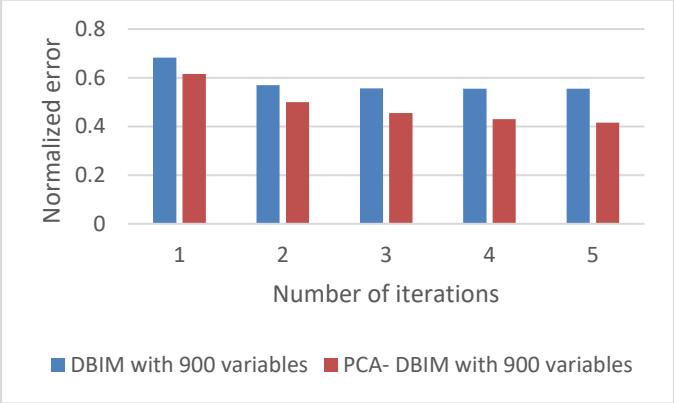

(c)

Fig. 5. Normalized reconstruction error over five iterations for DBIM and PCA-DBIM with 324 (a), 576 (b) and 900 (c) variables

Compared to traditional multi-frequency denoising strategies commonly employed in iterative ultrasound tomography [8], [12], [13], principal component analysis (PCA) offers several distinct advantages. Multi-frequency approaches rely on acquiring scattered data at multiple frequencies and integrating them to improve signal robustness and reduce noise artifacts. While effective, this technique often requires increased acquisition time, larger datasets, and additional computational effort due to the need for multiple forward and inverse simulations across frequency bands. Moreover, it assumes that the noise characteristics are frequency-independent and that the signal coherence across frequencies is high—conditions that are not always met in practice. In contrast, PCA operates directly on the spatial domain of the reconstructed signal, exploiting statistical redundancy within each iteration to isolate and preserve the most significant structural components. By decomposing the intermediate reconstruction into orthogonal principal directions, PCA efficiently discards low-variance components that are typically dominated by noise while retaining high-variance features associated with true anatomical structures. This intrinsic dimensionality reduction not only enhances noise suppression but also stabilizes the inversion pathway by preventing overfitting to noisy measurements. Furthermore, PCA is computationally lightweight and does not require modifications to the data acquisition protocol, making it particularly suitable for real-time or resource-constrained imaging systems. Unlike multi-frequency methods that aim to average out noise over several frequency-dependent reconstructions, PCA provides targeted noise rejection within each iteration, enabling faster convergence and improved reconstruction accuracy, even under severely underdetermined or high-noise conditions. This makes PCA-based filtering a robust and scalable solution for modern ultrasound tomography applications.

IV. Conclusions

In this work, we have developed and evaluated a PCA-regularized DBIM framework for ultrasound tomography, in which principal component analysis is embedded within each iteration of the image reconstruction process. By selectively preserving the dominant structural components of the intermediate solutions and filtering out low-variance noise elements, the proposed method effectively mitigates error propagation and accelerates convergence. Simulation results confirm that the PCA-enhanced DBIM consistently outperforms the conventional DBIM in terms of normalized reconstruction error—achieving relative error reductions of up to 36%—while requiring fewer iterations to reach a stable solution. This performance improvement is especially pronounced under underdetermined and noisy conditions, where standard DBIM tends to suffer from instability and slow progress. These findings highlight the potential of PCA as a lightweight yet powerful denoising mechanism that improves both accuracy and robustness in iterative acoustic image reconstruction, without introducing additional computational burden.

References

[1] C. F. Schueler, H. Lee, and G. Wade, ""Fundamentals of digital ultrasonic processing"," IEEE Transactions on Sonics and Ultrasonics, vol. 31, no. 4, pp. 195–217, July 1984.

[2] A. Kak and M. Slaney, Principles of Computerized Tomographic Imaging. Philadelphia, PA: SIAM, 2001.

[3] J. Greenleaf, J. Ylitalo, and J. Gisvold, ""Ultrasonic computed tomography for breast examination"," IEEE Engineering in Medicine and Biology Magazine, vol. 6, no. 4, pp. 27–32, December 1987.

[4] A. Devaney, ""Inversion formula for inverse scattering within the Born approximation"," Optics Letters, vol. 7, no. 3, pp. 111–112, March 1982.

[5] A. Devaney, ""Inverse-scattering theory within the Rytov approximation"," Optics Letters, vol. 6, no. 8, pp. 374–376, August 1981.

[6] W. C. Chew and Y. M. Wang, "Reconstruction of two-dimensional permittivity distribution using the distorted Born iterative method," IEEE Transactions on Medical Imaging, vol. 9, no. 2, pp. 218–225, June 1990.

[7] O. S. Haddadin, E. S. Ebbini, ""Solution to the inverse scattering problem using a modified distorted Born iterative algorithm"", Proceedings of IEEE Ultrasonics Symposium, pp. 1411-1414, 1995.

[8] R. Lavarello, M. Oelze, "Density imaging using a multiple-frequency DBIM approach", IEEE Trans UltrasonFerroelectrFreq Control, vol. 57, no. 11, pp. 2471-9, 2010. Doi: 10.1109/TUFFC.2010.1713.

[9] R. J. Lavarello and M. L. Oelze: Tomographic Reconstruction of Three-Dimensional Volumes Using the Distorted Born Iterative Method. IEEE Transactions on Medical Imaging, vol. 28, pp. 1643-1653, 2009.

[10] T. Tran-Duc, T. Nguyen-Linh, M. Do-Ngoc, ""Modified Distorted Born Iterative Method for Ultrasound Tomography by Random Sampling"", International Symposium on Communications and Information Technologies (ISCIT), 2012.

[11] R. Sloun, A. Pandharipande, M. Mischi, et al., ""Compressed Sensing for Ultrasound Computed Tomography"", IEEE Transactions on Biomedical Engineering, vol. 62, no. 6, pp. 1660-1664, 2015.

[12] S. Haddadin, Osama, and Ebbini Emad S., ""Multiple frequency distorted Born iterative method for tomographic imaging"", Acoustical Imaging, vol. 23, pp. 613-619, 1997.

[13] S. Haddadin, Osama, and Ebbini Emad S., ""Imaging strongly scattering media using a multiple frequency distorted Born iterative method"", IEEE Transactions on Ultrasonics, Ferroelectrics, and Frequency Control, vol. 45, no. 6, pp. 1485-1496, 1998.

[14] M. Zhenzhuang, and P. Kosmas, "Multiple-frequency DBIM-TwIST algorithm for microwave breast imaging", IEEE Transactions on Antennas and Propagation, vol. 65, no. 5, pp. 2507-2516, 2017.

[15] S. Yutaro, and S. Kidera, "Resolution Enhanced Distorted Born Iterative Method Using ROI Limiting Scheme for Microwave Breast Imaging", IEEE Journal of Electromagnetics, RF and Microwaves in Medicine and Biology, vol. 5, no. 4, pp. 379-385, 2021.